Journal of Econometrics and Statistics
Vol. 3, Issue 2, 2023, pp. 141-156
https://doi.org/10.47509/JES.2023.v03i02.03

A Reduced Form Approach for Modeling Credit Risk Sensitivity to Excessive CO2 Emissions

Djibril Gueye*[a]

[a]*Laboratoire de recherche et développement QUANTLABS: the innovative subsidiary of the RAINBOW PATERNS, a consulting firm specializing in Banking and Insurance, in financial services and IT professions, 8 rue Euler 75008, Paris, France.*

This paper presents a simulation study of a generalized Cox approach for modeling credit risk in the context of a firm exposed to extrem CO_2 emissions. The study uses a Poisson process to model the random events associated with such excessive CO_2 emissions, and a shot noise process to capture the impact of these emissions exceedances exceedances on the firm's hazard process. The simulations show the effectiveness of the generalized Cox approach in capturing the impact of extrem CO_2 emissions exceedances on credit risk, and the sensitivity of the results to changes in the model parameters.

keywords: credit risk, Emissions Trading System, GHGs, default probability.

1 Introduction

The current issue at hand focusses on the impact of emissions exceedances on a company's credit risk, which is particularly relevant in the context of the Emissions Trading System (ETS). The ETS, as a market-based mechanism, plays a significant role in addressing emissions and can have implications for a company's financial stability, regulatory compliance, and reputation. Under the ETS, companies are allocated emission allowances, which represent the authorization to produce or emit a specific quantity

*djibril.gueye@quantlabs.fr

Article History
Received : 20 August 2023; Revised : 5 September 2023; Accepted : 22 September 2023; Published : 30 December 2023

To cite this paper
Djibril Gueye (2023). A Reduced Form Approach for Modeling Credit Risk Sensitivity to Excessive CO2 Emissions. *Journal of Econometrics and Statistics.* 3(2), 141-156.

of greenhouse gases (GHGs). If a company exceeds its allocated allowances, it must purchase additional allowances from the market or face penalties and fines for non-compliance. When a company exceeds its emission allowances, it not only incurs financial penalties but also risks damaging its financial stability. The purchase of additional allowances can significantly impact profitability and cash flow, as the cost of allowances adds to operating expenses. Moreover, the need for costly remediation efforts or investments in emission reduction projects further strains financial resources, potentially affecting credit risk (see, e.g., Ellerman and Joskow (2008), Stavins (2008), Schaefer et al. (2010), Ellerman et al. (2016), Zheng et al. (2021)).

In the context of regulatory compliance, emissions exceedances can result in legal ramifications and reputational damage, both of which have implications for credit risk. Regulatory agencies closely monitor companies' compliance with their allocated allowances and may impose stricter monitoring and reporting requirements on those with a history of exceedances. This increased regulatory scrutiny heightens the risk of non-compliance, negatively impacting a company's solvency and creditworthiness Campiglio et al. (2018).

To illustrate the effects of emissions exceedances on financial health, several concrete examples can be highlighted. One prominent case is the Volkswagen emissions scandal in 2015. The company deliberately installed software in its diesel vehicles to manipulate emissions tests, resulting in significantly excessive CO_2 emissions. This misconduct led to substantial fines, legal settlements, and severe reputational harm for Volkswagen, thereby negatively affecting its solvency and market position (see, e.g., Jung and Sharon (2019) and the references theirin for more details on the Volkswagen emissions scandal).

Roughly speaking, emissions exceedances pose a significant issue with far-reaching implications for a company's credit risk. The financial implications, regulatory risks, and reputational consequences need to be carefully evaluated by companies to assess their environmental performance, mitigate risks, and enhance long-term financial viability.

In this paper we propose to adapt a particular case of the Generalized Cox model developed in Gueye and Jeanblanc (2022) to assess the impact of climate change on credit risk. Specifically, we aim to estimate the sensitivity of default probability to changes in macroeconomic factors, such as the excedances emissions CO_2 given a fixed threshold value defined by a potential regulatory compliance. Our approach falls within the range of bottom-up approaches, which involve individually assessing each credit or potential borrower to determine their level of risk. Traditionally, in the context of studying climate change effect in credit risk, the structural model with the Merton model has been widely used, as demonstrated in notable works such as Resilience et al. (2018); Capasso et al. (2020); Bouchet and Le Guenedal (2020); Bourgey et al. (2022).

However, we distinguish ourselves from other articles by adopting a reduced-form model. Unlike the structural model, which can be complex and require specific data on the assets and liabilities of borrowers, the reduced-form model simplifies the analysis by using more aggregated and easily accessible variables. This allows us to obtain results more quickly and efficiently when assessing credit risk associated with climate change.

To our knowledge, the reduced-form approach has not been previously employed in the evaluation of climate risk in credit risk. Our paper represents a pioneering effort in this regard. By adopting a reduced-form model, we aim to explore a novel approach to

assessing the impact of climate risk on credit risk.
By embarking on this research, we aim to contribute to the understanding of climate-related credit risk and pave the way for further investigations into the application of reduced-form models in this domain. Through our pioneering efforts, we hope to provide valuable insights and stimulate future research in assessing climate risk in credit risk using a reduced-form approach.

As mentioned earlier, our construction represents a specific model derived from the generalized Cox model (see Gueye and Jeanblanc (2022)). This model aims to address a limitation of the classical Cox model commonly used in the field of credit risk. In the traditional reduced-form approach, the modeling of defaults often excludes the occurrence of events that coincide with stopping times of a reference filtration. This limitation renders these models unsuitable for accurately modeling certain financial products exposed to default risk in the presence of external shocks . In such cases, there is a possibility that the default time may be equal, with a strictly positive probability, to one of the shock times that correspond to stopping times of the reference filtration. The generalized Cox construction aims to overcome this issue by proposing a model that incorporates these stopping times of the reference filtration, thereby enabling a more precise and realistic modeling of default risk in these specific contexts.

In Gueye and Jeanblanc (2022), a comprehensive theoretical framework and concrete examples were presented. This article, along with Chaieb and Gueye (2022), which specifically explores CAT bonds, significantly enhances the potential applications of this model in the domain of credit risk within the context of climate change.

The paper is structured as follows. In Section 2, we present our construction and methodology, with a specific focus on how our model is developed within the context of credit risk associated with CO_2 emission exceedances. We provide a comprehensive explanation of the methodology used to integrate CO_2 emissions into our model and analyze their impact on credit risk. In Section 3, we present the results of numerical experiments conducted to assess the efficiency and effectiveness of the model. We discuss the findings from these experiments and provide a detailed analysis of the model's performance in relation to CO_2 emissions and credit risk.

2 Methodology

2.1 Our model

We aim to model the default risk of a company that is exposed to high levels of CO_2 emissions which can have an impact on its credit risk. To achieve this, we adopt a modeling approach that involves the CO_2 emissions exceedance times of the company, denoted by an increasing sequence of stopping times $(\theta_i)_{i\geq 1}$, where $\tau_0 = 0$. These stopping times represent the occurrence of jumps in a homogeneous Poisson process N with an intensity of λ^N. Each of these exceedance times $(\theta_i)i \geq 1$ corresponds to a quantity of CO_2 emissions exceedance, represented by a sequence of independent and identically distributed (i.i.d) positive random variables $(y_i)i \geq 1$ supposed to be independent to N. It is important to note that these exceedances do not necessarily lead to the default of

the company, but they increase the probability of default. To incorporate the effect of these exceedances on the default probability, we introduce a shot noise process into the company's hazard process. This means that the hazard process of the company reacts to a jump of size $\rho(y_i)$ at the time of the i-th emissions exceedance, where ρ is a positive increasing function. Therefore, we define H as:

$$H_t := \Lambda_t + \sum_{i=1}^{N_t} \rho(y_i) e^{\alpha(t-\theta_i)}, \tag{2.1}$$

where $\Lambda_t := \int_0^t \lambda_s ds$ represents the cumulative hazard process without taking into account the climate change risk. Here, λ is a positive process adapted to a filtration $\mathbb{F}^W$ generated by a standard Brownian motion W, which is independent of the Poisson filtration $\mathbb{F}^N$. The parameter α is a positive constant that determines the decay rate of the impact of each emissions exceedance.

By incorporating the shot noise process into the hazard process, we can capture the increased risk of default associated with the CO_2 emissions exceedances. The Poisson process N analysis that accounts for the impact of CO_2 emissions exceedances can be interpreted as a process that models the random events associated with the company's CO_2 emissions. The intensity λ^N represents the average frequency of CO_2 emissions exceedances by the company, that is, the number of CO_2 emissions exceedances per unit time on average. This Poisson process N can be seen as a source of risk for the company because it generates random events that can influence the company's CO_2 emissions exceedances and hence its credit risk. For example, if λ^N is high, it means that the company emits frequently large amounts of CO_2 that exceed a fixed threshold level, which can increase its credit risk due to the negative impact on the environment and potential regulations. The weighting function $\rho(y_i)e^{\alpha(t-\theta_i)}$ refers to the factor by which each individual emission exceedance quantity, represented by y_i, contributes to the overall hazard process. The weight determines the importance or influence of a specific emission exceedance event on the resulting credit risk measure. It is determined by the combination of two components: $\rho(y_i)$ and $e^{\alpha(t-\theta_i)}$ which can be interpreted as follows:

a) The component $\rho(y_i)$ captures how the emission exceedance value itself influences the hazard process. The specific form of ρ will depend on the chosen function, such as linear, quadratic, or another mathematical relationship. The purpose of this component is to assign a weight to each emission exceedance quantity based on its magnitude or other relevant factors. Throughout this paper, we suggest to build this component on the following transformation based on commonly used class of functions called power functions: $\rho(y_i) = y_i^p$ where $p > 0$ that controls the sensitivity of the weights to the emissions. By adjusting the value of p, we can achieve different weighting characteristics:
   - If $p = 1$, ρ is linear. This means that the weights are directly proportional to the emissions, reflecting a direct impact of emissions exceedances on credit risk.

- If $0 < p < 1$, the relationship between exceedance quantities and credit risk is weakened. The credit risk may be less sensitive to the magnitude of exceedances.
- If $p > 1$, the impact of CO_2 emissions exceedances on credit risk increases at an accelerating rate. In other words, larger emissions exceedances have a disproportionately greater effect on credit risk compared to smaller exceedances. By means this amplifies the influence of large CO_2 emissions exceedances on credit risk. As a result, the credit risk increases more rapidly in response to extreme events.

b) The component $e^{\alpha(t-\theta_i)}$ introduces a time decay factor into the weighting function. It incorporates the time difference between the observation time t and the emission exceedance event time θ_i. The term $(t - \theta_i)$ represents the time elapsed since the emission exceedance event occurred. The exponential function $e^{\alpha(t-\theta_i)}$ determines how the weight assigned to an emission exceedance event diminishes as more time passes. The parameter α controls the rate at which the weight decreases over time. A higher α leads to a faster decay of the weight, while a lower α results in a slower decay.

By multiplying these two components together, the overall weight for each emission exceedance event is obtained. The larger the weight, the greater the impact of the corresponding emission exceedance on the credit risk measure.
Given the setup (2.1), we define the default time τ of the company as

$$\tau := \inf\{t \geq 0 : H_t \geq \Theta\} \tag{2.2}$$

with Θ an exponential random variable with parameter 1 independent of $\mathbb{F}$ where $\mathbb{F} = \mathbb{F}^W \vee \mathbb{F}^N$. This definition of default time is known as the Generalized Cox approach as studied in Gueye and Jeanblanc (2022).

2.2 Information flow representation

In this study, we suppose that the filtration $\mathbb{F}$ satisfies the usual conditions of naturalness and completeness and we consider the filtered probability space $(\Omega, \mathcal{F}, \mathbb{P}, \mathbb{F})$. We denote by $\mathbb{G}$ the enlargement of $\mathbb{F}$ with respect to the default time τ, i.e, $\mathcal{G}_t = \mathcal{F}_t \vee \sigma(\tau \leq s)$, for any $t \geq 0$.
Intuitively, this means that the filtration $\mathbb{G}$ contains all the information available in the filtration $\mathbb{F}$, as well as all the information related to the default time τ that has been revealed up to a certain time t. In other words, the enlarged filtration $\mathbb{G}$ represents the smallest filtration containing all the information available in $\mathbb{F}$, as well as all the information related to the default time that has been revealed up to a certain time t.
To study the conditional laws of τ, the chosen filtration must be rich enough to contain all relevant information about the default time τ. In general, the filtration $\mathbb{G}$ is useful for evaluating derivative products related to the default time τ hence is used to study the conditional laws of τ. Indeed, this filtration contains all available information in $\mathbb{F}$

as well as all information about the default time that has been revealed up to a certain time t.
Note in this study that the default time τ depends on macroeconomic factors such as CO_2 emissions, it may be necessary to choose the filtration $\mathbb{F}$ that contains information about these factors. However, as the filtration $\mathbb{F}$ is included in the extended filtration $\mathbb{G}$ with the default time τ, all the information available in $\mathbb{F}$ is also present in $\mathbb{G}$. Therefore, studying the conditional laws of τ in the filtration $\mathbb{G}$ is at least as accurate as doing so in the filtration $\mathbb{F}$. Therefore, here we choose the filtration $\mathbb{G}$ that is rich enough to capture all relevant information for the analysis of the conditional laws of τ even if we always need the projections of some $\mathbb{G}$-adapted processes onto $\mathbb{F}$ that are very useful for pricing.

2.3 Necessary quantities associated to the default time τ

In what follows we consider λ to be the following CIR square root diffusion process

$$d\lambda_t = \gamma(\theta - \lambda_t)dt + \sigma\sqrt{\lambda_t}dW_t, \qquad \lambda_0 = x,$$

where γ, θ, and σ are positive parameters. Hence we have, for any $0 \leq t \leq T$, the following known expression

$$Q_t(T) := \mathbb{E}\left[e^{-\int_t^T \lambda_s ds}|\mathcal{F}_t^W\right] = e^{A_t(T) - B_t(T)\lambda_t} \tag{2.3}$$

where A and B verify (see, e.g., Maghsoodi (1996)) $A_t(T) = 2\frac{\gamma\theta}{\sigma^2}\ln\left(\frac{2h\ e^{\frac{1}{2}(\gamma+h)(T-t)}}{h-\gamma+e^{h(T-t)}(h+\gamma)}\right)$ and $B_t(T) = \frac{-2(e^{h(T-t)}-1)}{h-\gamma+e^{h(T-t)}(h+\gamma)}$, where $h = \sqrt{\gamma^2+2\sigma^2}$.
We also assume that the random variables $(\rho(y_i))_i$ have the common cumulative distribution function F with density denoted by f_y. Therefore by denoting μ the random jump measure of the marked point process $(\theta_i, \rho(y_i))_{i\geq 1}$, i.e., $\mu(dt, dx) = \sum_{i\geq 1}\delta_{(\theta_i,\rho(y_i))}(dt, dx)$ where δ is the Dirac delta function located at $(\theta_i, \rho(y_i))$, μ admits the deterministic compensator compensator measure ν verifying $\nu(dt, dx) = \lambda^N F(dx)dt$. We denote by $\widetilde{\mu}$ the compensated random measure $\widetilde{\mu} = \mu - \nu$.

Lemma 2.1. *The $\mathbb{G}$-conditional survival probability of the firm is given, for any $0 \leq t \leq T$, by*

$$\mathbb{P}(\tau > T|\mathcal{G}_t) = \mathbb{1}_{\{\tau>t\}}Q_t(T)\frac{c(T)L_t(T)}{c(t)L_t(t)}, \tag{2.4}$$

where Q is given in (2.3), for any $0 \leq T$,

$$c(T) = \exp\big(\int_0^T\int_{\mathbb{R}}(e^{-\rho(x)e^{\alpha(T-s)}} - 1)\nu(ds, dx)\big)$$

and $L(T)$ is the $\mathbb{F}^N$-martingale given by

$$L_t(T) = \mathcal{E}(\int_0^t\int_{\mathbb{R}}\big(e^{-\rho(x)e^{\alpha(T-s)}} - 1\big)\widetilde{\mu}(ds, dx))$$

where $\mathcal{E}(X)$ denotes the Doléans-Dade exponential of the stochastic process X (i.e, for X being a càdlàg semimartingale then

$$\mathcal{E}(X)_t = e^{X_t - \frac{1}{2}\langle X^{(c)}, X^{(c)}\rangle_t} \prod_{0<s\leq t} (1+\Delta X_s)e^{-\Delta X_s},$$

where $X^{(c)}$ is the continuous martingale part of X.

Proof: This can be proved by first using a consequence of the Key Lemma 1 (see, e.g., Jeanblanc et al. (2009), Lemma 7.4.1.1), i.e.,

$$\mathbb{P}(\tau > T|\mathcal{G}_t) = \mathbb{1}_{\{\tau>t\}} \frac{\mathbb{E}[Z_T|\mathcal{F}_t]}{Z_t}$$

where Z is the Azéma surpermartingale given by $Z_t = e^{-H_t}$, and then from the fact that $\mathbb{F}^W$ independent to $\mathbb{F}^N$, one has

$$\mathbb{E}[e^{-H_T}|\mathcal{F}_t] = \mathbb{E}[e^{-\int_0^T \lambda_s ds}|\mathcal{F}_t^W]\,\mathbb{E}[e^{-\sum_{i=1}^{N_T}\rho(y_i)e^{\alpha(t-\theta_i)}}|\mathcal{F}_t^N]$$

hence

$$\begin{aligned}\mathbb{P}(\tau > T|\mathcal{G}_t) &= \mathbb{1}_{\{\tau>t\}}\mathbb{E}[e^{-\int_t^T \lambda_s ds}|\mathcal{F}_t^W]S_t(T)\\ &= \mathbb{1}_{\{\tau>t\}}Q_t(T)S_t(T)\end{aligned}$$

where

$$S_t(T) = \frac{\mathbb{E}[e^{-\sum_{i=1}^{N_T}\rho(y_i)e^{\alpha(t-\theta_i)}}|\mathcal{F}_t^N]}{e^{-\sum_{i=1}^{N_t}\rho(y_i)e^{\alpha(t-\theta_i)}}}$$

and finally the result follows by applying Proposition 3.18 in Gueye and Jeanblanc (2022) for computing $S_t(T)$.

From Lemma 2.1, the default probability associated to τ is given for any $u \geq 0$ by

$$\mathbb{P}(\tau \leq u) = 1 - Q_0(u)c(u).$$

Due to the markovian property of the particular shot noise (see Schmidt (2017) for more details about the markovian property of a shot noise process) used here, the result (2.1) can be written in a very closed form. Indeed, for $s \leq t \leq T$, one has $\rho(x)e^{\alpha(T-s)} = \rho(x)e^{\alpha(T-t)}e^{\alpha(t-s)}$ hence by simple computations using $L_t(T) = \exp(-\int_0^t\int_{\mathbb{R}}\rho(x)e^{\alpha(T-s)}\mu(ds,dx) - \int_0^t\int_{\mathbb{R}}(e^{-\rho(x)e^{\alpha(T-s)}}-1)\nu(ds,dx))$, it is not difficult to show the following equality

$$\mathbb{P}(\tau > T|\mathcal{G}_t) = \mathbb{1}_{\{\tau>t\}}Q_t(T)\exp\left(\int_t^T\int_{\mathbb{R}^+}(e^{-\rho(x)e^{\alpha(T-s)}}-1)\nu(ds,dx) - (e^{\alpha(T-t)}-1)Y_t\right), \tag{2.5}$$

where Y is the shot noise part of H, i.e, $Y_t := \sum_{i=1}^{N_t}\rho(y_i)e^{\alpha(t-\theta_i)}$, for any $t \geq 0$.

Therefore, by using the parameters about the CO2 emissions, we have

$$\begin{aligned}\mathbb{P}(\tau > T|\mathcal{G}_t) &= \mathbb{1}_{\{\tau>t\}} Q_t(T) \exp\left(\lambda^N \int_t^T \int_{\mathbb{R}^+} (e^{-\rho(x)e^{\alpha(T-s)}} - 1)F(d\rho(x))ds - (e^{\alpha(T-t)} - 1)Y_t\right) \\ &= \mathbb{1}_{\{\tau>t\}} Q_t(T) \exp\left(\lambda^N \int_t^T \left(\phi(e^{\alpha(T-s)}) - 1\right) ds - (e^{\alpha(T-t)} - 1)Y_t\right) \quad (2.6)\end{aligned}$$

where $\phi(u)$ is the Laplace transform of the distribution F evaluated at $u \in \mathbb{R}^+$, i.e, $\phi(u) = \int_{\mathbb{R}^+} e^{-uy} f_{\rho(X)}(y)dy$ with $f_{\rho(X)}$ the density function of $\rho(X)$.

Hence, the default probability of τ is given for any $u \geq 0$ by

$$\mathbb{P}(\tau \leq u) = 1 - Q_0(u) \exp\left(\lambda^N \int_0^u \left(\phi(e^{\alpha(u-s)}) - 1\right) ds\right). \quad (2.7)$$

Remark 2.2. Note that in some cases the Laplace transform may not exist in a closed form, meaning that it cannot be expressed using a finite combination of elementary functions. However it can still be calculated using numerical methods, such as numerical integration or series expansions.

3 Data and numerical analysis

The described model can be utilized in credit risk analysis by incorporating CO_2 emissions exceedances as an additional factor influencing the default risk of a company. In this section, we demonstrate our construction by utilizing projected data on CO_2 emissions. We apply our methodology to analyze and model CO_2 emissions based on the provided projections. Our study focuses on integrating CO_2 emissions exceedances as an additional factor impacting the default risk of a company. To simplify the analysis, we assume the idiosyncratic component to be zero (i.e., $\lambda = 0$). In a more practical setting, this component can be calibrated using market CDS spreads. By calibrating the model with more realistic data, we can consider the unique characteristics of different entities and achieve a more accurate assessment of the default risk associated with CO_2 emissions.

3.1 Data

The dataset consists of historical emissions data for the years 2017 to 2021, which were collected from an anonymous company operating in the aviation industry sector. This publicly traded corporation specializes in painting airplanes. These emissions data represent the total amount of CO2 emitted by the company in each respective year, categorized into scopes 1, 2, and 3, and measured in metric kilotons (kt) of CO2. Recognizing the limitations arising from insufficient data for our study, we propose the creation of hypothetical projection scenarios as a means to enhance our dataset. By generating these

projections, we aim to simulate potential future emissions and expand our dataset for a more comprehensive analysis. To construct the dataset, we applied a degraded scenario, assuming a gradual increase in emissions over time. By incorporating a random pattern into the projections, we introduced variability and uncertainty into the simulated emissions. This approach allows us to explore potential trends and outcomes for the company's emissions in the future. The projections were generated by multiplying the average emissions of the previous years by a random factor between 1.0 and 1.2. This range of variation accounts for different potential growth rates and ensures a diverse set of scenarios within the optimistic framework. The projected emissions cover a period of 50 years, from the initial year of 2022 to the final year of 2071.
The resulting dataset (see Table 1) includes the projected year and the corresponding emissions for each year. These projections, although hypothetical, provide valuable insights into potential future emissions trends for the company. It's important to note that these projections are based on assumptions and random variation patterns and may not accurately represent actual future emissions. Nonetheless, they serve as a valuable tool for analysis, allowing us to explore different possibilities and assess the potential impact of various emission scenarios.

Year	CO_2 Emissions
2017	1,013,101.00
2018	959,825.00
2019	1,123,000.00
2020	900,000.00
2021	827,000.00
2022	1,266,211.20
2023	1,052,472.50
2024	1,334,925.60
2025	987,567.80
2026	1,080,798.20
2027	1,143,772.80
2028	1,257,043.60
...	

Table 1: Degraded projections of CO_2 Emissions (in kt) for the company

3.2 Numerical analysis

This section presents our simulation approach for assessing credit risk resulting from CO_2 emissions exceedances using the shot noise model. To accurately capture the dynamics of credit risk, we employ a comprehensive framework that incorporates various parameters and statistical techniques. First, we select a threshold based on the 95th

percentile of the CO_2 emissions data, specifically at 1,148,860 ts. This threshold represents a stringent limit, encompassing 95% of the emissions distribution while allowing for a small fraction of outliers or higher emissions. By setting this threshold, we ensure that our analysis focuses on the most significant exceedances.
To model the CO_2 emissions exceedances, we utilize the generalized Pareto distribution (GPD) with estimated parameters. The shape parameter (γ) is determined to be 0.01210418, and the scale parameter (β) is estimated as 3120.091 using the R package POT Ribatet (2007). These parameters enable us to accurately capture the tail behavior of the exceedances distribution. The frequency of exceedances is calculated by dividing the number of exceedances by the total number of time periods. This provides an estimate (λ^N) for the intensity parameter of a Poisson distribution fitted to the exceedances. In our case, we find λ^N to be 0.003, reflecting the average frequency of CO_2 emissions exceedances. For the simulation, we set the initial time period (t_0) to 0 and the simulation horizon (T) to 50 years. We perform 1000 simulations, dividing the simulation horizon equally among them to determine the timestep (δt). Setting the hazard process parameter (α) to 0.02, we account for the underlying hazard rate of credit risk. To simulate the magnitude of the jumps in the shot noise process, we employ the GPD parameters to generate the CO_2 emissions exceedances. Additionally, we set the power parameter (p), which governs the behavior of the shot noise process, to 0.1. These choices allow us to accurately represent the characteristics of credit risk arising from CO_2 emissions exceedances.
Using the aforementioned parameters, our simulation generates the shot noise process for the time interval from T to the simulation horizon. The output includes a time vector and a data frame containing the simulated credit risk values. Through our simulations, we have observed that the hazard process displays jumps precisely aligned with the jumps in the Poisson process, indicating CO_2 emissions exceedances. This finding emphasizes the direct influence of these exceedances on credit risk. Remarkably, these jumps in the hazard process significantly impact Azéma's supermartingale, resulting in corresponding negative jumps at the exact same moments. Figure 1 visually depicts this phenomenon, offering a clear illustration of the interplay among CO_2 emissions exceedances, the hazard process, and the behavior of Azéma's supermartingale.

Our simulation framework provides flexibility for scenario analysis and sensitivity testing. By adjusting parameters such as the threshold (λ^N), hazard process parameter (α), shape parameter (γ), scale parameter (β) and power parameter (p), we can explore various credit risk patterns and evaluate the effectiveness of risk management strategies.

3.2.1 Sensitivity of default probability to different parameter values

In the analysis, we focus on understanding how changes in the values of λ^N, α, the shape (γ), and scale (β) affect the default probability of a company. To conduct the analysis, we set the following parameter values: $p = 0.01$, $\lambda^N = 0.003$, $\alpha = 0.02$, $\beta = 3120.091$, and $\gamma = 0.01210418$. We also define a vector of maturities, including time periods of 5, 10, 15, and 20, which represent different time horizons for assessing default risk. By systematically varying these parameter values, we calculate the default probabilities for

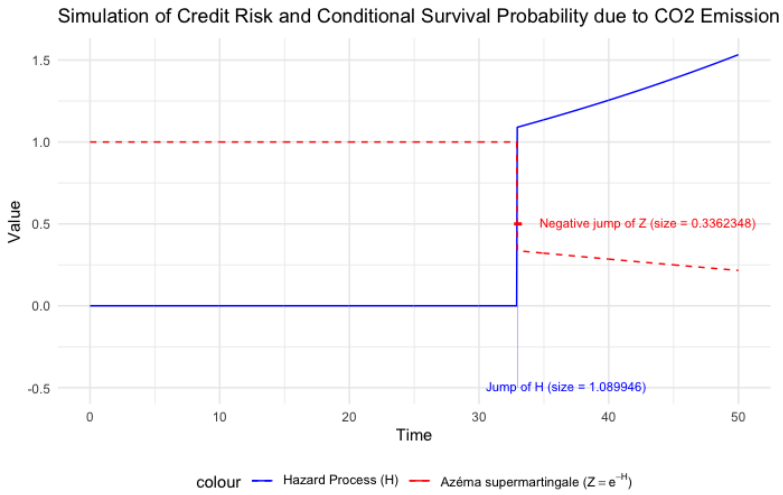

Figure 1: In blue, we observe a sample path of the hazard process given by Equation (2.1). In red, we have the Azéma supermartingale denoted by $Z = e^{-H}$. At time $t = 33$, a significant positive jump of magnitude 1.089946 occurs in the hazard process H. Consequently, we observe a corresponding negative jump of magnitude 0.3362348 in the Azéma supermartingale Z at the same moment.

each maturity. This allows us to observe how changes in these parameters influence the default risk over time. By iterating through the parameter values and updating the specified parameter, we calculate the default probabilities for each maturity. This allows us to observe how variations in these parameters impact the default risk over time. The selected parameter values cover a broad range of possible settings. By considering various combinations of parameter values within these ranges, we gain valuable insights into the sensitivity of default probability to changes in these parameters. Results of this analysis are showed in Figure 2. This figure consists of subfigures, each displaying a 2D plot representing the default probability with respect to a specific parameter.

In Subfigure 2(a), we explore the sensitivity of default probability to changes in the λ^N parameter. The plot displays the relationship between different λ^N values (ranging from 0.0001 to 0.05) on the x-axis and maturities (5, 10, 15, and 20) on the y-axis. The z-axis represents the sensitivity of default probability. The analysis reveals a consistent pattern: as λ^N increases, default probabilities also increase across all maturities. This indicates that a higher default intensity corresponds to a greater likelihood of default. The progressive increase in default probabilities demonstrates a positive relationship between λ^N and default risk. Furthermore, the impact of λ^N on default probabilities varies with the maturity of the financial instrument. For longer maturities, the effect of higher λ^N values on default probability becomes more significant compared to shorter maturities. This implies that changes in the default intensity have a stronger influence on long-term default risk. In other words, variations in λ^N have a more pronounced impact on default probability for extended time horizons. These findings underscore the criti-

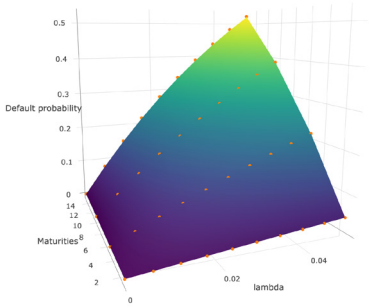

(a) Default Probability vs. λ^N and maturities

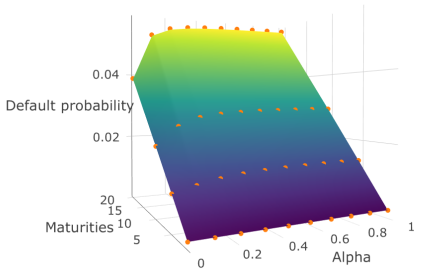

(b) Default Probability vs. α and maturities

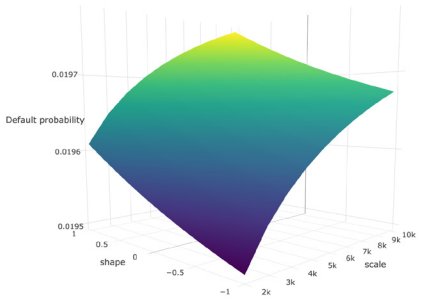

(c) Default Probability vs. Scale (γ) and Shape (β) Parameters for a Maturity of 10 Years

Figure 2: Default Probability Sensitivity Analysis: Impact of Parameters on Default Risk

cal importance of accurately estimating and monitoring the default intensity parameter (λ^N) when evaluating default risk. Higher λ^N values indicate an increased probability of default, particularly for longer maturities. Therefore, comprehending the sensitivity of default probability to changes in λ^N is essential for effective risk management and informed decision-making in financial contexts.

Subfigure 2(b) showcases the sensitivity of default probability with respect to the parameter α. The x-axis represents the values of α, ranging from 0.005 to 2, while the y-axis represents the maturities. The z-axis indicates the sensitivity of default probability. This plot allows us to analyze the impact of different the values of α on default probability over the specified maturities. For values of α close to zero, corresponding to longer maturities, we observe a rapid increase in default probabilities. This indicates that the impact of extreme events with very low values becomes more significant for longer time horizons when α is near zero. As α increases from zero, the default probabilities continue to rise, but at a slower pace. This suggests that extreme events still have an influence on default probabilities, but the effect becomes less pronounced as α deviates from zero. The rate of increase in default probabilities for α values greater than zero varies across maturities. While there is a general upward trend, the magnitude of the increase is more prominent for longer maturities. Notably, for very small values of α, the increase in default probabilities is particularly significant, indicating a higher vulnerability to extreme events and default risk for companies operating in such conditions. As α approaches higher values, the rate of increase in default probabilities diminishes, implying that extreme events have a lesser impact on default probabilities compared to lower values of α.

Subfigure 2(c) provides insights into the sensitivity of default probability to changes in the shape parameter, specifically for a maturity of 10 years. The x-axis represents the shape values, ranging from -1 to 3.5, while the y-axis represents the scale parameter, ranging from 2000 to 10000. The z-axis indicates the sensitivity of default probability. The analysis reveals that the shape parameter has a moderate impact on default probabilities. As the shape parameter increases, default probabilities also increase, indicating a higher level of default risk. Conversely, as the shape parameter decreases, default probabilities decrease, suggesting a lower default risk. In contrast, the scale parameter exerts a more pronounced influence on default probabilities. Larger values of the scale parameter lead to higher default probabilities, signifying an elevated default risk. Conversely, smaller values of the scale parameter result in lower default probabilities, indicating a reduced default risk. To summarize, both the shape and scale parameters play a role in determining default probabilities. However, the scale parameter has a more significant effect on the magnitude of default probabilities compared to the shape parameter.

3.2.2 Stress Testing Analysis Report for CO_2 Emission Management

In our study on CO_2 emission management, we conducted a stress testing analysis to assess the risks associated with exceeding emission thresholds. The primary objective

was to determine the value of lambda that corresponds to a target default probability for a specific emission threshold. This approach enables us to quantitatively evaluate the risk and implement appropriate measures to mitigate emissions. To perform the analysis, we made the following assumptions:

- The maturity period was fixed at 10 years.
- The parameter p of rho was set to p=0.01.
- We utilized a simplified model with $\alpha = 0$ to simplify the estimation process.

For the target default probability, we selected values ranging from 0.3% to 5% with a step size of 0.005%. This range covers a wide spectrum of risk levels and allows for a comprehensive assessment of the system's resilience. Regarding the emission thresholds, we set them at the following values: 975597.9, 1071825.1, 1134181.4, and 1151342.9. These thresholds represent critical points at which the risk of exceeding emissions is expected to be significant. To determine the value of λ^N corresponding to the target default probability for each threshold, we iterated over different values of λ^N until the calculated default probabilities matched the target default probabilities. For each value of λ^N, we calculated the probability corresponding to exceeding the emission threshold. By gradually adjusting the value of λ^N, we eventually found the value that corresponded to the target default probability for the fixed threshold. Based on the analysis, we obtained value of λ^Ns corresponding to the target default probabilities and thresholds. However, we have only included a selection of snapped values in Table 2. This table provides an overview of the values of λ^N obtained for different combinations of default probabilities and thresholds, offering insights into the risk levels associated with specific emission thresholds. Furthermore the results can be seen in Figure 3 consisting in a 2 D plot of the stressed values of λ^N with respect to the fixed thresholds and the target values. For example, when the target probability is set to 5% and the emission threshold is fixed at 1151342.9 units, we obtained a value of λ^N of 0.007826996. This value of λ^N can be interpreted as a measure of the risk level associated with the company's CO_2 emissions. A higher value of λ^N indicates a higher frequency of exceeding the emission threshold. In this case, a value of λ^N of 0.007826996 suggests that the company faces a relatively high risk of exceeding the 1151342.9-unit emission threshold.

Fixed Threshold	Target Default Probability	$\widehat{\lambda}^N_{\text{stress}}$
975597.9	0.03343333	0.005063629
1071825.1	0.03895556	0.005941772
1134181.4	0.04447778	0.006858826
1151342.9	0.05000000	0.007826996

Table 2: Stressed values of λ^N for Different Target Default Probabilities at maturity 10 years

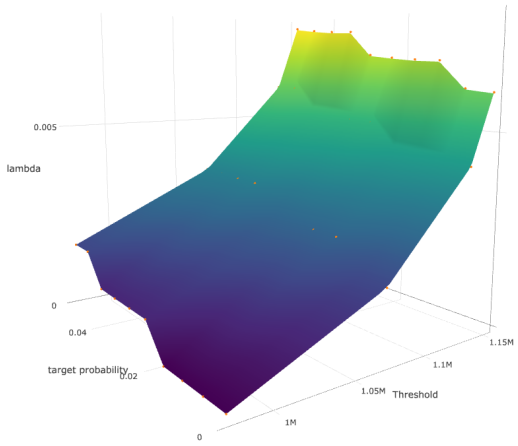

Figure 3: Stressed values of λ^N for Different Target Default Probabilities at maturity 10 years.

4 Conclusion

This paper represents a significant contribution to the literature on assessing the impact of climate change, particularly CO_2 emission exceedances, on credit risk for companies. By employing a reduced-form model derived from the Generalized Cox model developed in Gueye and Jeanblanc (2022), we were able to depart from more complex structural approaches and focus on aggregated and easily accessible variables. The conducted numerical experiments validated the efficiency and effectiveness of the model, enhancing our understanding of the sensitivity of default probability to changes in macroeconomic factors related to CO_2 emission exceedances. In this step, we explored some simulated scenarios of data from an aviation firm.

However, this pioneering work also raises exciting new questions and perspectives, including the distribution of emitted CO_2 excess quantities $(y_i)_i$, the form of the impact function ρ on the risk process, and the intensity λ^N of the Poisson process. Future improvements could involve exploring these aspects in greater depth and gaining a better grasp of the underlying mechanisms.

A more in-depth analysis of historical emissions data and the relationships between emissions exceedances and companies' financial performance would further enrich the model. Additionally, incorporating other factors related to climate change, such as the transition to renewable energy sources, would provide a more comprehensive view of the climate's impact on credit risk.

Improving this model could also involve considering the potential interactions between climate-related risks and other financial risks, as well as exploring the implications of different regulatory frameworks on credit risk. Furthermore, validating the model with real-world data from multiple companies and sectors would enhance its robustness and applicability.

References

Bouchet, V. and Le Guenedal, T. (2020). Credit risk sensitivity to carbon price. *Available at SSRN 3574486*.

Bourgey, F., Gobet, E., and Jiao, Y. (2022). Bridging socioeconomic pathways of co 2 emission and credit risk. *Annals of Operations Research*, pages 1–22.

Campiglio, E., Dafermos, Y., Monnin, P., Ryan-Collins, J., Schotten, G., and Tanaka, M. (2018). Climate change challenges for central banks and financial regulators. *Nature climate change*, 8(6):462–468.

Capasso, G., Gianfrate, G., and Spinelli, M. (2020). Climate change and credit risk. *Journal of Cleaner Production*, 266:121634.

Chaieb, Z. and Gueye, D. (2022). Pricing zero-coupon cat bonds using the enlargement of filtration theory: A general framework. *Journal of Mathematical Finance*, 12:582–605.

Ellerman, A. D. and Joskow, P. L. (2008). *The European Union's emissions trading system in perspective*. Pew Center on Global Climate Change Arlington, VA.

Ellerman, A. D., Marcantonini, C., and Zaklan, A. (2016). The european union emissions trading system: ten years and counting. *Review of Environmental Economics and Policy*.

Gueye, D. and Jeanblanc, M. (2022). Generalized cox model for default times. *Frontiers of Mathematical Finance*, 4(1):467–489.

Jeanblanc, M., Yor, M., and Chesney, M. (2009). *Mathematical methods for financial markets*. Springer Science & Business Media.

Jung, J. C. and Sharon, E. (2019). The volkswagen emissions scandal and its aftermath. *Global business and organizational excellence*, 38(4):6–15.

Maghsoodi, Y. (1996). Solution of the extended CIR term structure and bond option valuation. *Mathematical finance*, 6(1):89–109.

Resilience, A.-B. C. et al. (2018). Navigating a new climate: Assessing credit risk and opportunity in a changing climate-outputs of a working group of 16 banks piloting the tcfd recommendations part 2: Physical risks and opportunities.

Ribatet, M. (2007). Pot: Modelling peaks over a threshold. *R News*, (7):1.

Schaefer, M., Scheelhaase, J., Grimme, W., and Maertens, S. (2010). The economic impact of the upcoming eu emissions trading system on airlines and eu member states-an empirical estimation. *European Transport Research Review*, 2(4):189–200.

Schmidt, T. (2017). Shot-noise processes in finance. In *From statistics to mathematical finance*, pages 367–385. Springer.

Stavins, R. N. (2008). Addressing climate change with a comprehensive us cap-and-trade system. *Oxford Review of Economic Policy*, pages 298–321.

Zheng, Y., Sun, X., Zhang, C., Wang, D., and Mao, J. (2021). Can emission trading scheme improve carbon emission performance? evidence from china. *Frontiers in Energy Research*, 9:759572.